Study on Characteristics of Magnetostrictive Bistable Energy Harvester with Spring Oscillator

Mingliang Cai, Baiping Yan, Jianghuang Wang, Yuxi Lu, Hongyu Wu
School of Automation, Guangdong University of Technology, Guangzhou, Guangdong, China

Abstract: Monostable cantilever beam magnetostrictive energy harvester needs to operate at a specific intrinsic frequency, while the conventional magnetostrictive bistable energy harvester (CMBEH) with the introduction of a magnetic force has difficulty in forming the inter-trapping motion under weak excitation, which results in a narrow operating bandwidth. In order to broaden the operating bandwidth of the harvester and improve its output power, a magnetostrictive bistable energy harvester with an auxiliary spring oscillator (MBEH-SO) is proposed. Firstly, a coupled machine-magneto-electric model of MBEH-SO is established based on the intrinsic equations of magnetostrictive materials, Faraday's law of electromagnetic induction and the magnetic dipole model, and then the potential morphology, frequency scans and amplitude scans of the harvester are analyzed in detail numerically using this model, and the results show that the MBEH-SO possesses complex dynamic phenomena such as chaos, inter-trapping and intratrapolating motions. Compared with the conventional magnetostrictive bistable energy harvester, its effective bandwidth is increased by at least four times, the maximum average power generated can be up to 41.2 mW, and the excitation amplitude required to trigger the inter-trap motion can be reduced by up to 50%. Numerical simulation results show that the motion of the spring oscillator can provide additional kinetic energy for the cantilever beam to facilitate the escape of the potential trap, and its resonance effect can easily lead to the stable operation of the cantilever beam in a high-energy orbit, thus generating an independent operating bandwidth. MBEH-SO has the excellent performances of wide bandwidth, high power, and low threshold, which is conducive to the harvesting of energy from the low-frequency and weakly-excited environmental vibration.

Keywords: Magnetostrictive; Auxiliary Spring Oscillator; Bistable Energy Harvester; Effective Bandwidth

1. Introduction

With the rapid development of wireless sensors, implantable electronic devices and wearable devices, energy harvesting, as a clean and sustainable technology, can solve the shortcomings of batteries such as continuous charging, high maintenance cost and environmental pollution [1]. Therefore, energy harvesting technology based on environmental vibration has attracted wide attention from scholars. The main types of energy harvesting are electrostatic, electromagnetic, piezoelectric and magnetic elongation Contracted. The electrostatic type is small in size, but its power is very low, usually tens to hundreds of uW; Electromagnetic type can produce enough electric energy under strong magnetic field, but the weight and volume are relatively large; Piezoelectric type has the advantages of high energy conversion efficiency, easy realization and miniaturization, and is widely used in the conversion of mechanical energy to electric energy [2, 3]. However, the disadvantages of piezoelectric materials such as easy aging, high brittleness and low tensile strength limit its application. Magnetostrictive materials have the advantages of large mechanomagnetic coupling coefficient, high sensitivity, fast response speed, and solve the problems of depolarization, aging and brittleness. Magnetostrictive vibration energy harvesters made of materials with magnetostrictive effect [4, 5] have the advantages of good output characteristics, large energy density and high stability [6-8].

Magnetostrictive vibration energy harvesters are mainly divided into columnar and cantilever beam types. Among them, columnar

and rod vibration harvesters have high mechanical strength and stable structure, but they have some disadvantages such as large magnetoresistive loop, large magnetic leakage, low electromagnetic conversion efficiency and small output voltage [9]. The cantilever beam type has the advantages of high output efficiency, large output voltage and more sensitive to environmental vibration, and is mostly used for vibration energy collection under weak excitation (30~50N)[10-13]. Yoo [14] made a cantilever beam type vibration energy collector based on the magnetostrictive material Galfenol. In the experiment, it was measured that when the cantilever beam base was subjected to 1g acceleration and the frequency was stimulated at 222Hz, 2.2mW of power could be obtained, and the energy conversion efficiency exceeded 60%. Existing Galfenol cantilever beam collectors all adopt traditional linear cantilever beam structure, which can only produce high output power in a narrow resonant band [15]. However, environmental vibration is time-varying, low frequency and small amplitude, resulting in low operating bandwidth and poor environmental adaptability of traditional linear monostable magnetostrictive energy harvesters [16]. With the development of energy collector, scholars at home and abroad have proposed a bistable structure of magnetostrictive vibration energy collector, which has a wider operating bandwidth than linear monostable energy collector. Cao S [17] et al. designed a magnetostrictive bistable energy collector

Based on the magnetic dipole model, a lumped parameter model of the device is established. Simulation verifies that CMBEH can collect energy in a wider frequency band. Liu Lu [18] et al. designed a magnetostrobe bistable energy collector (NMVG+DEM) with elastic amplifier, determined the key parameters of the device, and verified by simulation that NMVG+DEM has low frequency and wide band characteristics. When the excitation amplitude is 2g, it can be used at 30-55Hz. The output voltage and power are obtained

Significantly improved, Liu H F [19] et al. designed a bistable magnetostrictive vibration energy collector with a displacement amplification structure. Through simulation and experiment, it was verified that the bistable structure could broaden the resonance band of the system, the displacement amplification structure could realize the amplification of the excitation level, and the maximum output voltage could reach 590mV. In general, the monostable magnetostrictive energy harvester only works at resonant frequencies for efficient energy harvesting. And the traditional bistable magnetostrictive energy The collector (CMBEH) can expand the working bandwidth of the device, but it has a fixed barrier, when the environmental energy is not enough to allow the device to escape the potential well, over the barrier, the collector can only vibrate near a stable equilibrium position, can not form a movement between the well for efficient energy Quantity collection.

Therefore, a kind of magnetostrictive bistable energy collector (MBEH-SO) with spring oscillator is proposed in this paper. The collector is optimized with spring vibrators, specifically when the base is excited, the movement of the spring vibrator provides additional kinetic energy to the cantilever beam to facilitate the escape of the potential well. When the cantilever beam resonates with the spring vibrator, the resonance of the spring vibrator directly acts on the end of the cantilever beam, making the main beam vibrator overcome the barrier and run on the high-energy track, thus generating an independent working bandwidth, which is conducive to collecting the low-frequency environmental energy. Based on the magnetostrictive nonlinear constitutive equation, Faraday's law of electromagnetic induction and magnetic dipole model, the MBEH-SO mechanical-magnetic-electrical coupling model is established. The numerical simulation analysis of the energy collector is carried out in detail. The results show that MBEH-SO has wide band, low threshold excitation and good power generation capacity.

2. The Structure and Mathematical Modeling of MBEH-SO

2.1 Structure of MBEH-SO

Figure 1 shows the structure diagram of CMBEH and MBEH-SO. The construction of the MBEH-SO consists of a cantilever beam and a spring vibrator component, as well as two permanent magnets, where the cantilever is made of a magnetostrictive material (Galfenol) layer bonded to aluminum sheets.

Two permanent magnets placed horizontally between the free end and the fixed end of the beam provide the Galfenol layer with a biased magnetic field Hb. The free end of the beam and the permanent magnet mounted on the spring vibrator are pointed at each other with the N-pole, causing magnetic repulsion between them. When the collector base is excited, the distance between the magnets A and B is dynamic, which makes the barrier or potential well not constant, which is affected by both the base excitation and each other's nonlinear magnetic force. Here we assume that magnet B only moves in the vertical direction and does not take into account the horizontal oscillation. Therefore, the dynamic behavior of the cantilever beam and the spring oscillator is tightly coupled. When the excitation frequency reaches a certain value, the resonance of the spring oscillator can provide additional kinetic energy for the cantilever beam to promote the escape of the potential well and trigger the motion between the well of the cantilever beam to further widen the working bandwidth. CMBEH has no spring oscillator, the distance between magnets A and B is fixed, and it has a fixed barrier and potential well.

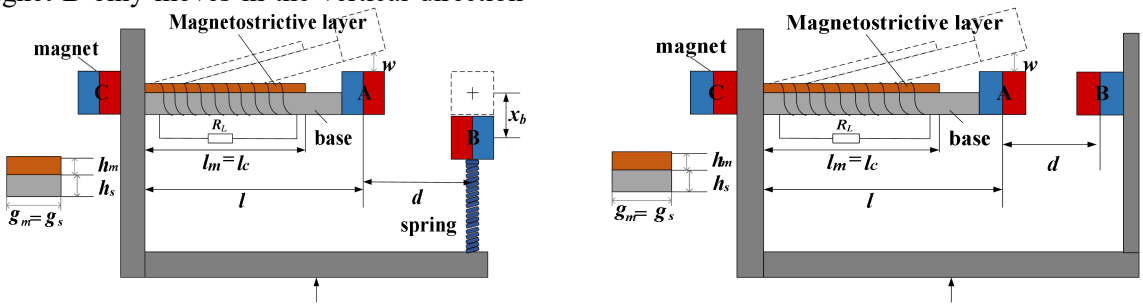

(a). MBEH-SO Structure Diagram **(b). CMBEH Structure Diagram**

Figure 1. Structure Diagram of Two Energy Harvesters

2.2 Magnetic Model

The geometric relationship between magnet A and magnet B is shown in Figure 2. According to the magnetic dipole principle, their magnetic moment vectors can be written as:

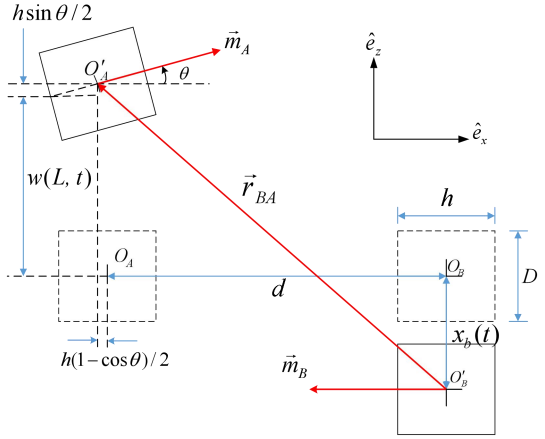

Figure 2. Geometry of the Magnetic Dipole Model

$$\boldsymbol{m}_A = M_A V_A \left(\cos\theta \boldsymbol{e}_x + \sin\theta \boldsymbol{e}_z\right) \quad (1)$$

$$\boldsymbol{m}_B = -M_B V_B \cos\theta \boldsymbol{e}_x \quad (2)$$

Where, M_A and M_B are the magnetization intensity of magnet A and B respectively ($M=Br/\mu_0$,Br is the residual magnetic flux density, μ_0 is the permeability constant). V_A、V_B are the volume of magnet A and B ($V=h\pi D^2/4$), θ is the deflection Angle of magnet A.

The direction vector from magnet B to magnet A is:

$$\boldsymbol{r}_{BA} = -\left(d + \frac{h}{2} - \frac{h}{2}\cos\theta\right)\boldsymbol{e}_x + \left(w + \frac{h}{2}\sin\theta + x_b\right)\boldsymbol{e}_z \quad (3)$$

d is the horizontal distance between the center of magnet A and the center of magnet B when it is in the horizontal initial position. θ is the deflection Angle of permanent magnet A after the beam vibration, $w(l,t)$ is the vertical displacement of A, and $x_b(t)$ is the vertical displacement of B.

The magnetic induction intensity generated by magnet B on magnet A is:

$$\boldsymbol{B}_{BA} = -\frac{\mu_0}{4\pi}\nabla\frac{\boldsymbol{m}_B \cdot \boldsymbol{r}_{BA}}{\|\boldsymbol{r}_{BA}\|_2^3} \quad (4)$$

Where, ∇denotes the vector gradient operator, and $\|\ \|_2$ denotes the binary norm

Then the magnetic potential energy between magnet B and magnet A is:

$$U_m = -\boldsymbol{B}_{BA} \cdot \boldsymbol{m}_A = \frac{\mu_0}{4\pi}\left[\frac{\boldsymbol{m}_B}{\|\boldsymbol{r}_{BA}\|_2^3} - (\boldsymbol{m}_B \cdot \boldsymbol{r}_{BA}) \cdot \frac{3\boldsymbol{r}_{BA}}{\|\boldsymbol{r}_{BA}\|_2^5}\right] \cdot \boldsymbol{m}_A \quad (5)$$

From (5) :

$$U_m = \frac{\mu_0 M_A V_A M_B V_B \left[(2K_2^2 - K_1^2)\cos\theta - 3K_1K_2\sin\theta\right]}{4\pi(K_1^2 + K_2^2)^{\frac{5}{2}}} \quad (6)$$

The magnetic repulsion force of the system can

be obtained from the upper differential:

$$\boldsymbol{F_m} = \frac{3\mu_0 M_A V_A M_B V_B \left[\hat{\boldsymbol{r}}_{BA}(\hat{\boldsymbol{\mu}}_A \cdot \hat{\boldsymbol{\mu}}_B) + \hat{\boldsymbol{\mu}}_A(\hat{\boldsymbol{r}}_{BA} \cdot \hat{\boldsymbol{\mu}}_B)\right]}{4\pi \left\|\boldsymbol{r}_{BA}\right\|_2^4} + \frac{3\mu_0 M_A V_A M_B V_B \left[\hat{\boldsymbol{\mu}}_B(\hat{\boldsymbol{r}}_{BA} \cdot \hat{\boldsymbol{\mu}}_A) - 5\hat{\boldsymbol{r}}_{BA}(\hat{\boldsymbol{r}}_{BA} \cdot \hat{\boldsymbol{\mu}}_A)(\hat{\boldsymbol{r}}_{BA} \cdot \hat{\boldsymbol{\mu}}_B)\right]}{4\pi \left\|\boldsymbol{r}_{BA}\right\|_2^4} \quad (7)$$

The hat symbol represents the unit vector, and the orthogonal decomposition of $\boldsymbol{F}_{\mathrm{m}}$ along the coordinate axis gives the vertical magnetic force subject to magnet A:

$$F_{mz} = \frac{3\mu_0 M_A V_A M_B V_B}{4\pi (K_1^2 + K_2^2)^{\frac{7}{2}}} \left[(K_1^2 + K_2^2)(K_2 \sin\theta - K_1 \cos\theta)\right] + \frac{3\mu_0 M_A V_A M_B V_B \left[5K_1 K_2 (K_2 \cos\theta - K_1 \sin\theta)\right]}{4\pi (K_1^2 + K_2^2)^{\frac{7}{2}}} \quad (8)$$

Among

$K_1=w(l,\mathrm{t})+h\sin\theta/2+x_{\mathrm{b}}(t)$，$K_2=d+h(1-\cos\theta)/2$.

2.3 MBEH-SO Mechanical-Magnetic-Electrical Coupling Model

The constitutive equation of the magnetostrictive material Galfenol is shown as follows

$$\varepsilon = \sigma_m / E_m + d_1 H \quad (9)$$

$$B = d_1 \sigma_m + \mu H \quad (10)$$

Where: ε is strain; σ_{m} is stress; E_{m} is the Young's modulus of Galfenol; H is the magnetic field strength where Galfenol is located; Bias field strength for permanent magnets A and C; N is the number of coil gates wrapped around Galfenol; i is coil current; l_{c} is the length of the solenoid; B is the magnetic induction intensity; μ is the permeability of Galfenol; At that time,H=3580A/m piezomagnetic coefficient d_1 could be written as [17]:

$$d_1 = G_0 / E_m \times \exp\left[-\left(\varepsilon \times 10^6 + b_0\right)^2 / \left(2c_0^2\right)\right] \quad (11)$$

Where $G_0 = 2432$; $b_0 = 248.6$; $c_0 = 193.9$; the strain ε is as follows:

$$\varepsilon(x) = 3h\left(x - l\right)w / l^3 \quad (12)$$

Where $x = 0.65l$; l is the effective length of the cantilever beam; h is the distance from the neutral axis of the cantilever beam to the center of Galfenol; w is the relative displacement of the cantilever tip.

If the tip displacement w=0 and the bias magnetic field H_{b}=0, the constitutive equation can be simplified as:

$$\sigma_{mi} = -E_m d_1 N i / l_c \quad (13)$$

The current stress is as follows:

$$\sigma_{mi} = \frac{1}{\left(h_m + h_s\right) l_m} \int_0^{l_m} \int_0^{h_m + h_s} \frac{F_i\left(l - x\right)}{I_b} z dz dx = \frac{F_i\left(2l - l_m\right)\left(h_m + h_s\right)}{4 I_b} \quad (14)$$

where h_m and l_m are the thickness and length of Galfenol, respectively; h_s is the thickness of the substrate; F_i is the reaction force generated by the current; $I_b = \left[g_s\left(h_b^3 - h_a^3\right) + g_m\left(h_c^3 - h_b^3\right)\right] / 3$ is the moment of inertia of the cross-sectional area; h_a, h_b and h_c are the distances from the neutral axis to the bottom of the substrate, the bottom of Galfenol and the top of Galfenol, respectively.

Make the above equation equal:

$$\frac{-E_m d_1 N i}{l_c} = \frac{F_i\left(2l - l_m\right)\left(h_m + h_s\right)}{4 I_b} \quad (15)$$

The expression for the force F_i associated with current i can be given as:

$$F_i = -d_1 k_i i \quad (16)$$

where $k_i = 4E_m I_b N / [\left(2l - l_m\right)\left(h_m + h_s\right) l_c]$.

According to the constitutive relation model of Galfenol and the expression of strain:

$$B = 3d_1 E_m h\left(x - l\right)w / l^3 + \left(\mu - d_1^2 E_m\right)\left(H_b + Ni / l_c\right) \quad (17)$$

According to Faraday 's law of electromagnetic induction, the induced voltage generated in the coil is as follows:

$$\Delta u = -\Delta l_c N S_c \dot{B} / l_c \quad (18)$$

where l_c is the coil length; $S_c = g_m h_m$ is the cross-sectional area of magnetostrictive material. Combined Eq. (8) and Eq. (9) can be obtained: $u = \beta \dot{w} - L_c \dot{i}$. When the coil resistance is R_c and the external circuit resistance is R_L, the voltage drop can be expressed as: $u = \left(R_L + R_c\right) i = Ri$. Combining the above equations, the electrical port equation can be obtained as follows:

$$\beta \dot{w} - L_c \dot{i} - Ri = 0 \quad (19)$$

where $\beta = 3d_1 N S_c E_m h\left(2l - l_m\right) / \left(2l^3\right)$; $L_c = \left(\mu - d_1^2 E_m\right) N^2 S_c / l_c$.

The nonlinear equivalent model of MEBH-SO lumped parameters is shown in Figure 3.

where $m_e = M_t + 33m / 140$ is the equivalent mass of the cantilever beam; $c_e = 2\zeta (k_e m_e)^{1/2}$ is the equivalent damping of cantilever beam; ζ is the damping ratio of cantilever beam;

$k_e = 3EI_b / l^3$ is the equivalent stiffness of the cantilever beam; $EI_b = \left[g_s E_s \left(h_b^3 - h_a^3 \right) + g_m E_m \left(h_c^3 - h_b^3 \right) \right] / 3$ is the average stiffness; m_B is the equivalent mass of the spring vibrator ; c_B is the equivalent damping ratio of the spring vibrator; k_B is the equivalent stiffness of the spring oscillator.

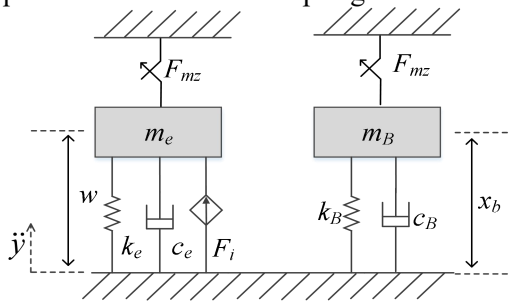

Figure 3. MBEH-SO Centralized Parametric Nonlinear Equivalent Modeling

When the acceleration of the base vibration is $\ddot{y} = a\sin(\omega t)$, according to the MBEH-DB lumped parameter nonlinear equivalent model in Fig. 3, the mechanical-magnetic-electric coupling model is obtained as follows:

$$\begin{aligned} &m_e\ddot{w}(t) + c_e\dot{w}(t) + k_e w(t) - F_{mz} - F_i = -m_e\ddot{y}(t) \\ &m_B\ddot{x}_b(t) + c_B\dot{x}_b(t) + k_B x_b(t) + F_{mz} = -m_B\ddot{y}(t) \\ &\beta\dot{w} - L_c\dot{i} - Ri = 0 \end{aligned} \quad (20)$$

3. Numerical Simulation Analysis

In this paper, the relevant material properties of the collector are referred to [14], as shown in Table 1. To compare the performance of the two collectors, this article sets the parameters of MBEH-SO and CMBEH to the same value.

3.1 Potential Energy form Analysis

For MBEH-SO, the potential energy function U of the system is [20]:

$$U = \frac{1}{2}k_e w^2 + \frac{1}{2}k_b {x_b}^2 + U_m \quad (21)$$

For U, set x_b to 0 and ignore the effect of the spring oscillator, which is the potential energy of CMBEH. Through numerical calculation, the potential energy surface of MBEH-SO and the potential energy curve of CMBEH can be obtained, as shown in Figure 1.

Table 1.Simulation Parameters

Parameter	Sign	value
Galfenol		
Length	l_m	38 mm
Width	g_m	6.35mm
Thickness	h_m	0.76 mm
Young's modulus	E_m	70GPa
Magnet		
Cantilever and magnet A mass	me	10.34g
Mass of magnet B	m_B	29g
Volume of magnet A	V_A	1080mm^3
Volume of magnet B	V_B	1080mm^3
Aluminum		
Length	l_s	58mm
Width	g_s	6.35mm
Thickness	h_s	1.27 mm
Young's modulus	E_s	68GPa
Miscellaneous		
Damping ratio of beam	ζ	0.014
Spring stiffness	k_b	8000N/m
Load resistance	R_L	100Ω
Number of coil gates	N	1000

The results show that the barrier of MBEH-SO and CMBEH decreases with the increase of magnetic distance d. When d=8mm and 9mm, the MBEH-SO potential energy surface presents two asymmetric potential barriers separated by oblique potential barriers, which is the sign of a bistable system. With the change of x_b, the potential well and potential barrier of MBEH-SO are changing, while the curve of CMBEH has a fixed potential well and potential barrier. When d increases to 10mm and 11mm, the bistable characteristics of MBEH-SO and CMBEH slowly disappear and almost become monostable structures, and the magnetic effect is very weak. Therefore, the bistable characteristics of MBEH-SO are obviously different from those of CMBEH. The asymmetric barrier is an obvious feature of MCBEH-SO.

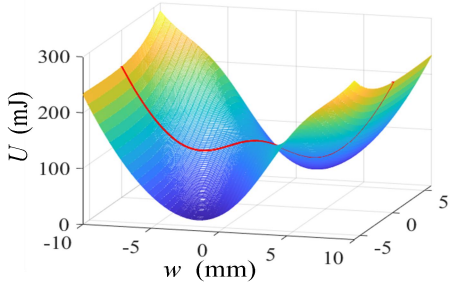

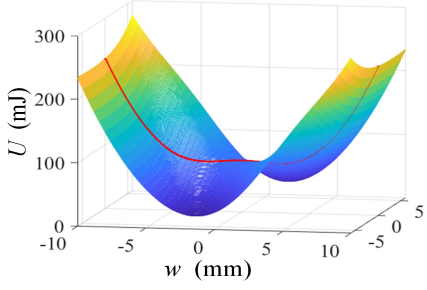

(a) d=8mm (b)d=9mm

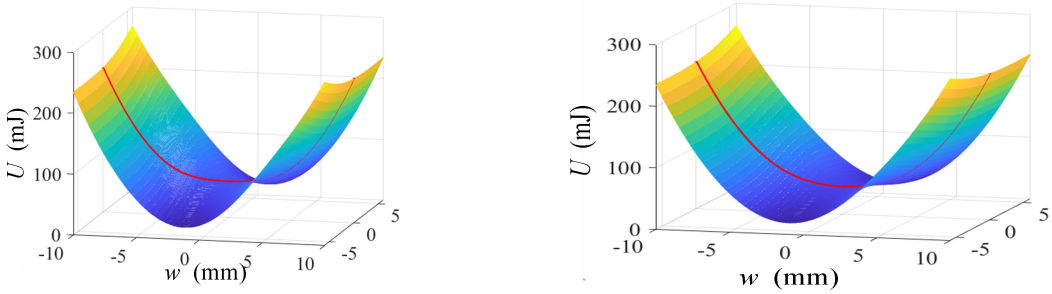

(c)d=8mm (d)d=9mm

Figure 4. Potential Energy Surfaces for Different Magnetic Distances MBEH-SO and Potential Energy Curves for CMBEH

3.2 Sweep Frequency Analysis

To compare the energy harvesting bandwidth and power generation performance of MBEH-DB and CMBEH. A numerical simulation frequency scanning analysis was carried out, and the scanning frequency function was shown in equation (21) :

$$\ddot{y} = A\sin\left(\Omega_0 + \Omega_r t / 2\right)t \tag{22}$$

Where: A is the acceleration amplitude; Ω_0 is the initial frequency; Ω_r is scanning rate is 0.05 Hz/s.

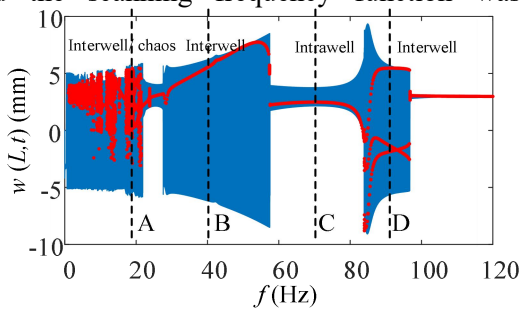

(a) MBEH-SO Tip Displacemen

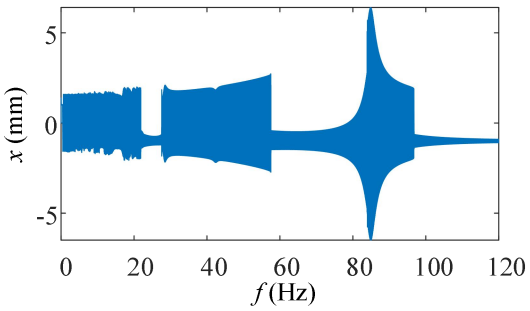

(b) Spring Oscillator Displacement

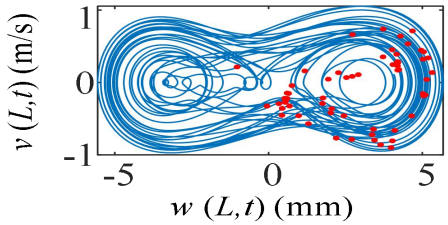

(c) Phase Diagram at A

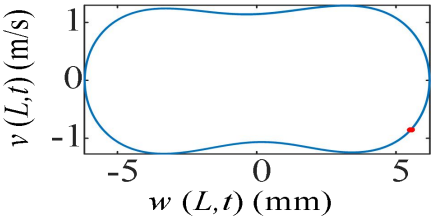

(d) Phase Diagram at B

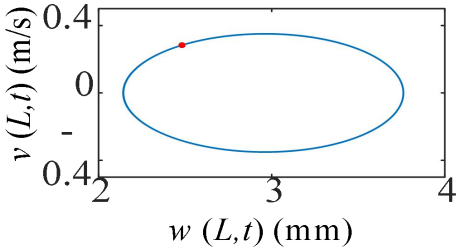

(e) Phase Diagram at C

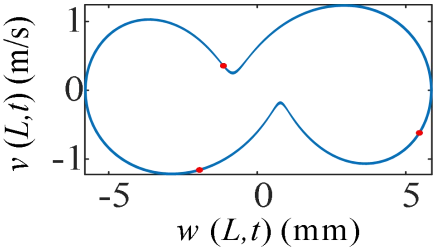

(f) Phase Diagram at D

Figure 5. MBEH-SO Forward Frequency Sweep at 2g Excitation

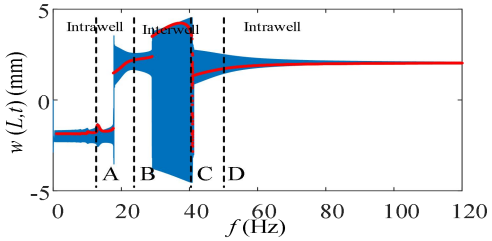

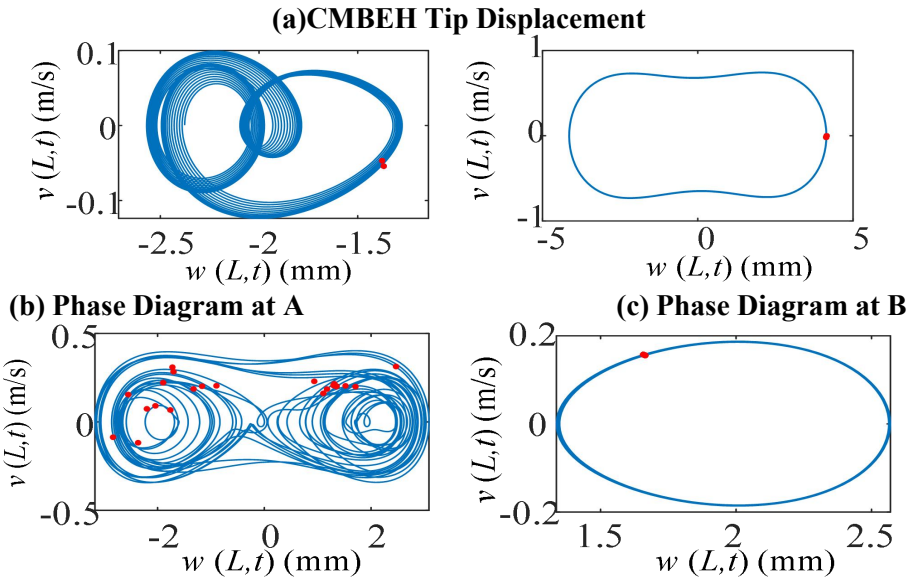

Figure 6. CMBEH Forward Frequency Sweep at 2 g Excitation

Fig. 5(a) and Fig. 6(a) respectively show the dynamic response of the tip of MBEH-SO and CMBEH when A=2g; Fig. 5(c-f) and Fig. 6(b-e) are their phase diagrams respectively; the points in red are Poincare mappings. As can be seen from Figure 5(a), the cantilever tip of MBEH-SO undergoes a complex dynamic process. At low frequencies, chaotic motion dominates, and the corresponding phase diagram is shown in Figure 5(c), where Poincare is mapped as disordered points. At 21.7Hz, it enters the orbit in the well, and at 28.3Hz, it begins to work stably in the orbit between the well across the two barriers. The Poincare map has only one point, and the dynamic response of the tip is single-period motion. When the frequency is 57.2Hz, the response suddenly jumps down to the inner trap track. However, as the excitation frequency is further increased, the auxiliary spring oscillator enters its resonance region, as shown in Figure 5(b). Under the action of auxiliary spring oscillator resonance, when the frequency is 82.8Hz, the response again enters the high energy orbit between the Wells, and finally at 96.3Hz, the response enters the low energy orbit between the Wells. MBEH-SO has an amplitude of 4.1-5.8mm in chaotic motion and a bandwidth of 21.7Hz (0-21.7Hz). The amplitude of the motion region between the first well is about 5.6-8.5mm, and its bandwidth is about 29.8Hz (27.7-57.5Hz). The amplitude of the motion region between the second well is 5.2-9.0mm, and its bandwidth is about 12.7Hz (84.0-96.7Hz).

It can be seen from Figure 6 (a) that in most frequency ranges, the tip displacement of the cantilever beam of CMBEH is captured by the inner well track, and only in the frequency band 29.2~40.8 Hz, there is movement between the Wells.

Based on the above analysis, a simple summary can be made. For MBEH-SO, it has several high-energy motion modes, such as chaotic motion (0 to 21.7 Hz), and interwell motion (27.7 to 57.5Hz and 27.7 to 57.5Hz). For CMBEH, there is only one high energy mode of motion (29.2~40.8 Hz) between the Wells. Therefore, under the forward sweep frequency of 2g, the effective bandwidth of MBEH-SO is 64.2Hz, while that of CMBEH is 11.6 Hz, which is about 1/6 of MBEH-SO.

To better evaluate the output power of MBEH-SO and CMBEH, the instantaneous power and average power are defined as:

$$P = v_{out}(t)^2 / R_L \tag{23}$$

$$P_a = \frac{1}{T_S}\int_0^{T_S} \frac{v_{out}^2(t)}{R_L} dt = \frac{1}{N_S R_L}\sum_{i=1}^{N_S} v_{out}^2(i),\ \ (i = 1,2,\cdots N_S) \tag{24}$$

Where, *Ts* is the sampling period; *Ns* is the number of sampling points.

Figure 7 depicts the power generated on the load RL when A=2g. The blue line indicates instantaneous power and the red line indicates average power per second. It can be seen that the output instantaneous power waveform is similar to the displacement response of the tip

of the cantilever beam. Average power is used to evaluate the output power. Combined with Figure 8, it can be seen that under 2g excitation, the maximum average power of MBEH-SO is 41.2mW, while the maximum average power of CMBEH is 10.2mW (about 25% of MBEH-SO). Obviously, both MBEH-SO and CMBEH have relatively high average power operating in the intertrap orbit. In addition, compared with CMBEH, the average power corresponding to the mixed motion of MBEH-SO and the motion between the second well caused by the resonance of the spring oscillator is still quite considerable. For example, when the excitation frequency enters the spring resonance region (about 82.8Hz), the maximum average power of MBEH-SO is 37.1mW, while the maximum average power of CMBEH is only 0.06mW, which is much smaller than MBEH-SO. It is worth mentioning that the low frequency range corresponding to the chaotic motion (0-21.7Hz) belongs to the effective bandwidth of MBEH-SO, and the maximum average power is also 5.7mW, which indicates that it is conducive to obtaining low frequency vibration energy from the environment that CMBEH does not have.

In addition, the effective bandwidths of two energy harvesters with different excitation amplitudes are also studied. Figures 9 and 10 show the dynamic response of the collector in frequency scanning for two hours at A=1.5g and A=2.5g.

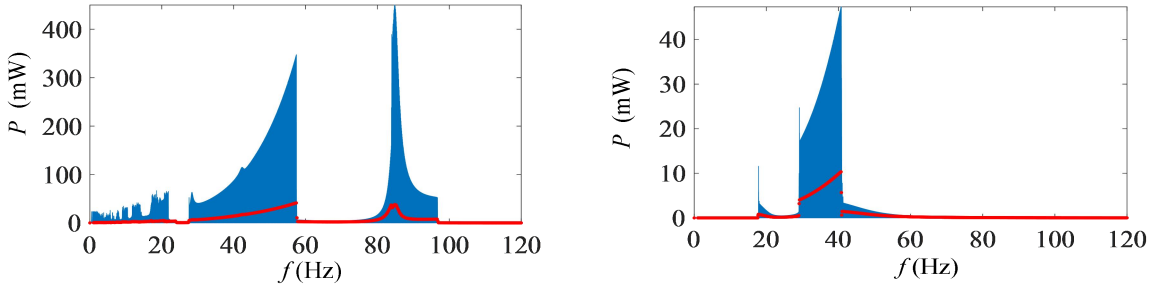

(a) Power of MBEH-SO **(b) The power of CMBEH**

Figure.7 Power of Two Collectors with Forward Sweep at 2g Excitation

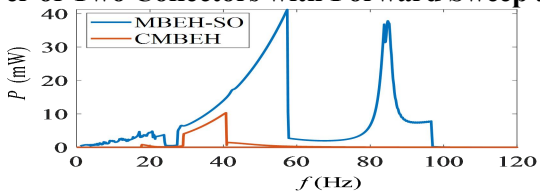

Figure 8. MBEH-SO and CMBEH Average Power under 2g Excitation

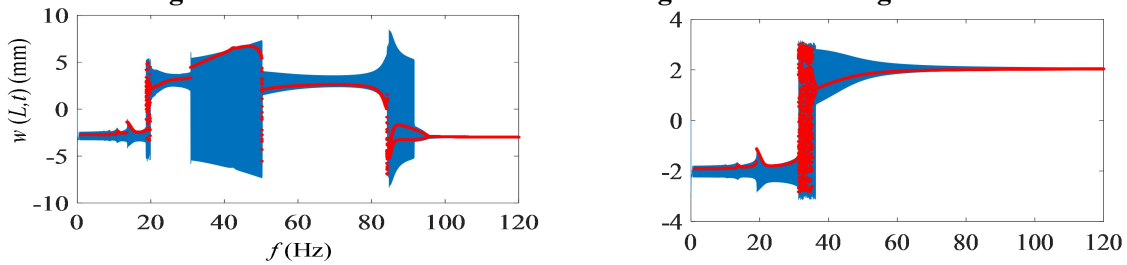

(a) MBEH-SO Dynamic Response **(b) CMBEH Dynamic Response**

Figure 9. Forward Frequency Scanning Cantilever Beam Tip Displacement at 1.5 g Excitation

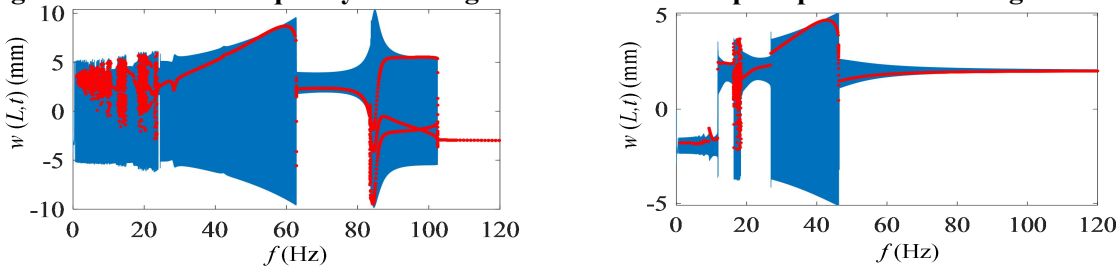

(a)MBEH-SO Dynamic Response **(b)CMBEH Dynamic Response**

Figure 10. Forward Frequency Scanning Cantilever Beam Tip Displacement at 2.5 g Excitation

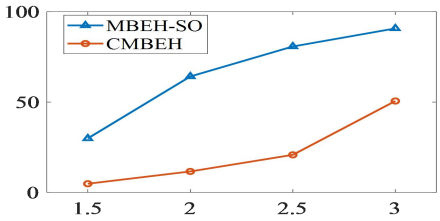

Figure 11. MBEH-SO and CMBEH Effective Bandwidth Statistics for Different Incentive Levels

Fig.9 and Fig. 10 show the dynamic response of the two collectors in the sweep frequency when the excitation amplitude is 1.5g and 2.5g respectively. It can be seen that when A=1.5g, the effective bandwidth of MBEH-SO is 29.9Hz, while that of CMBEH is 4.8Hz, about 16% of MBEH-SO.When A=2.5g,the effective bandwidth of MBEH-SO is 80.8Hz, while that of CMBEH is 20.8Hz, which is about 26% of that of MBEH-SO. Combined with Figure 11, it can be seen that with the increase of excitation amplitude, not only the amplitude of the two energy harvesters becomes larger, but also the efficiency bandwidth becomes wider. However, under the same excitation conditions, MBEH-SO always has larger amplitude and wider effective bandwidth than CMBEH. This is because the motion of the spring vibrator provides additional energy to the cantilever beam, and when the resonance of the spring vibrator helps to promote the cantilever's potential well to escape into the tracks between the Wells, additional independent bandwidth is generated.

3.3 Sweep Analysis

In order to compare the excitation threshold required for MBEH-SO and CMBEH to enter the high energy orbit between the trap. The amplitude scanning analysis of numerical simulation is carried out, and the scanning function is shown in equation (25) :

$$\ddot{y} = (A_0 + A_r t)\sin(\Omega t) \tag{25}$$

Where Ω,A_0 and A_r are excitation frequency, initial excitation amplitude and sweep speed ($0.05m/s^2/S$), respectively.

Figure 12 shows the dynamic response of the two collectors in the forward amplitude scanning when the excitation frequency is 20Hz. In forward amplitude scanning, once the amplitude exceeds $15.0m/s^2$, MBEH-SO moves from the in-trap orbit to the inter-trap orbit, and CMBEH responds similarly to MBEH-SO with a corresponding amplitude of $29.9m/s^2$. The results show that at low frequencies, MBEH-SO only needs about $15.0m/s^2$ to escape the barrier, while CMBEH needs about $29.9m/s^2$. FIG. 13 shows the dynamic response of the two kinds of collectors during forward amplitude scanning when the excitation frequency is 40 Hz. It can be seen that the excitation level of MBEH-SO at $10.4m/s^2$ enters chaotic motion from the inter-trap track, and the excitation level at $19.3m/s^2$ transitions to the high-energy orbit between the traps. The response of CMBEH is also similar to that of MBEH-SO, but the corresponding amplitudes are $22.8m/s^2$ and $39.8m/s^2$, respectively. Fig.14 shows the dynamic response of the two collectors during forward amplitude scanning when the excitation frequency is 60 Hz. At this time, an excitation level of $31.8m/s^2$ is required for MBEH-SO to enter into the chaotic motion between the well, while CMBEH has reached $52.5m/s^2$. The results show that the excitation threshold required for MBEH-SO to enter the well is lower than that of CMBEH, no matter it is under low frequency, medium frequency or high frequency excitation frequency. This is because when the cantilever beam and the spring vibrator are excited together, the movement of the spring vibrator provides additional kinetic energy to the cantilever beam end to promote the escape of the potential well head, making it easier for MBEH-SO to operate in the high-energy orbit between the Wells, an advantage that is unique to MBEH-SO, but not CMBEH.

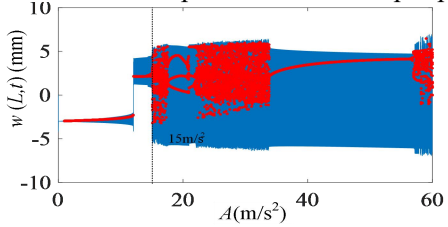

(a)MBEH-SO Dynamic Response

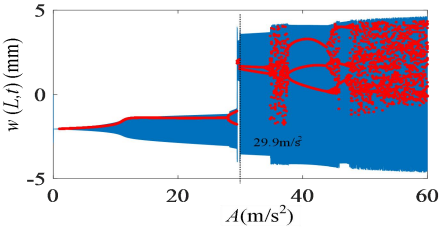

(b)CMBEH Dynamic Response

Figure 12. Forward Amplitude Scanning Cantilever Beam Tip Displacement at an Excitation Frequency of 20 Hz

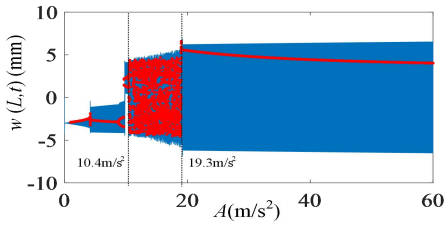

(a)MBEH-SO Dynamic Response

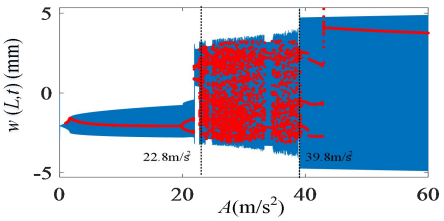

(b)CMBEH Dynamic Response

Figure 13. Forward Amplitude Scanning Cantilever Beam Tip Displacement at an Excitation Frequency of 40 Hz

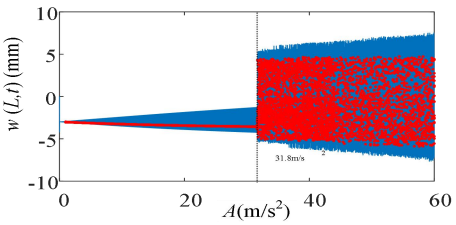

(a)MBEH-SO dynamic response

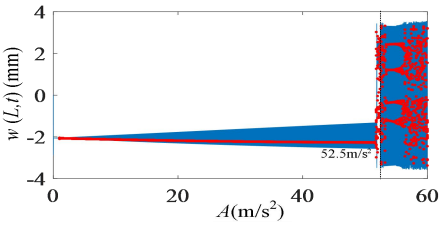

(b)CMBEH dynamic response

Figure 14. Forward Amplitude Scanning Cantilever Beam Tip Displacement at An Excitation Frequency of 60 Hz

4. Conclusion

In this paper, a kind of magnetostrictive bistable energy collector with spring oscillator is proposed. Under the action of magnetic force, the motion of the spring oscillator can effectively improve the dynamic characteristics of the cantilever beam, thereby reducing the excitation threshold, expanding the working bandwidth and increasing the output power. Based on the constitutive equation of magnetostrictive material, Faraday's law of electromagnetic induction and magnetic dipole model, the mechanical-magnetic-electrical coupling model of MBEH-SO is established. Combined with nonlinear dynamics, the potential energy form, frequency sweep and amplitude sweep of the collector are analyzed numerically. The results show that MBEH-SO has complex dynamic phenomena such as chaos, motion between and within the trap. For forward frequency scanning with an excitation amplitude of 2g, the effective bandwidth of MBEH-SO is 64.2Hz, while that of CMBEH is 11.6 Hz, which is about 1/6 of MBEH-SO. MBEH-SO has a maximum average power of 41.2mW, while CMBEH has a maximum average power of 10.2mW (about 25% of MBEH-SO). In addition, the excitation threshold required for MBEH-SO to enter the trap is lower than that of CMBEH at both low frequency, medium frequency and high frequency excitation frequencies. Therefore, this new type of magnetostrictive bistable energy collector with spring oscillator has the excellent performance of wide band, high power and low threshold, which is conducive to collecting energy from low frequency and weak excitation environmental vibration, and has great application prospects.

References

[1] Cui Shuhui, Zhou He, Huang Zhenxing, et al. An overview of key technologies and applications of power batteries for secondary utilization. Guangdong Electric Power,2023,36(01):9-19.

[2] Zheng Youcheng, Zhu Guoqiang, Liu Zhoulong, et al. Characterization of an asymmetric, variable potential energy trap tri-stable piezoelectric vibration energy harvester. Journal of Vibration Engineering,2023,36(05):1280-1291.

[3] Han Minglei. Dynamic characterization of directionally adaptive piezoelectric energy harvester. Jilin University,2023.

[4] Liu Zhen, Tang Wei, Xu Weihong, et al. Measurement and simulation of hysteresis and magnetostrictive coupling characteristics of core silicon steel. New Technology of Electrical Engineering,2024,43(05):1-9.

[5] Feng Yuelei, Liu Yang, Li Lin,et al. Simulation and experimental study on vibration of amorphous alloy three-dimensional coiled core considering magnetostriction effect. New Technology of Electrical Engineering and

Electricity,2022,41(03):15-22
[6] Wu Xun. Design and characteristic analysis of magnetostrictive tristable vibration collection system. Shenyang University of Technology,2023.
[7] Wan Dong, Liu Huifang, Zhang Jing, et al. Research on magnetostrictive vibration energy harvesting method for rotating environment. Mechanical Science and Technology,2021,40(04):604-608.
[8] He Zhongbo, Bai Guo, Xue Guangming, et al. Research progress of magnetostrictive vibration energy recovery technology. Machine Tools and Hydraulics,2019,47(05):144-150.
[9] Liu H F, Zhao X X, Liu H A, Yang J X, Magnetostrictive biomechanical energy harvester with a hybrid force amplifier, International Journal of Mechanical Sciences, Volume 233,2022,107652.
[10] Chen L, Liao X, Sun B, Zhang N, WU J. A numerical-experimental dynamic analysis of high-efficiency and broadband bistable energy harvester with self-decreasing potential barrier effect. Appl Energy 2022;317.
[11] Liang H, Hao G, Olszewski OZ. A review on vibration-based piezoelectric energy harvesting from the aspect of compliant mechanisms. Sens Actuators, A 2021;331: 112743.
[12] Huang Wenmei, Liu Zequn, Guo Wanli, et al. Fully coupled nonlinear equivalent circuit model of magnetostrictive vibration energy harvester. Journal of Electrotechnology,2023,38(15):4076-4086.
[13] Zhao Luyao, Liu Huifang, Late Dong. Design and characterization of magnetostrictive rotating energy harvester with double beam structure. Journal of Sensing Technology,2023,36(04):529-535.
[14] Yoo, J.-H.; Flatau, A B. A bending-mode galfenol electric power harvester. Journal of Intelligent Material Systems and Structures,2012, 23(6),647–654.
[15] Cong C. Analysis of influencing factors and optimization design of cantilever magnetostrictive vibration energy collector. Shenyang University of Technology,2021.
[16] Wang Guangqing, Liao Wei-Hsin. Dynamic and energetic characteristics of a bistable piezoelectric vibration energy harvester with an elastic magnifier. Mech Syst Signal Process 2018;105:427–46.
[17] Cao S ,Sun S , Zheng J , et al. Modeling and analysis of Galfenol cantilever vibration energy harvester with nonlinear magnetic force. Aip Advances, 2018, 8(5):05671.
[18] Liu Lu. Research on nonlinear wide-band magnetostrictive vibration generator and its energy management control circuit. Hebei University of Technology,2019.
[19] Liu H F, Zhao L Y, Chang Y L, Cong C. Design and characteristic analysis of magnetostrictive bistable vibration harvester with displacement amplification mechanism. Energy Conversion and Management 2021;243:114361.
[20] Liu H, Cong C, Cao C, Zhao Q. Analysis of the key factors affecting the capability and optimization for magnetostrictive iron-gallium alloy ambient vibration harvesters. Sensors 2020, 20, 401.

